BBA - Molecular Basis of Disease 1870 (2024) 167033

Contents lists available at ScienceDirect

BBA - Molecular Basis of Disease

journal homepage: www.elsevier.com/locate/bbadis

The striking differences in the bioenergetics of brain and liver mitochondria are enhanced in mitochondrial disease

Valeria Balmaceda [a], Timea Komlódi [b,e], Marten Szibor [c,d], Erich Gnaiger [e], Anthony L. Moore [f,*,1], Erika Fernandez-Vizarra [a,g,**,1], Carlo Viscomi [a,g,**,1]

[a] Department of Biomedical Sciences, University of Padova, Padova, Italy
[b] Department of Biochemistry and Molecular Biology, Semmelweis University, Budapest, Hungary
[c] Department of Cardiothoracic Surgery, Center for Sepsis Control and Care (CSCC), Jena University Hospital, Friedrich Schiller University of Jena, Jena, Germany
[d] Faculty of Medicine and Health Technology, Tampere University, Tampere, Finland
[e] Oroboros Instruments, Schöpfstr. 18, 6020 Innsbruck, Austria
[f] Biochemistry & Biomedicine, School of Life Sciences, University of Sussex, Brighton BN1 9QG, UK
[g] Veneto Institute of Molecular Medicine, Padova, Italy

ARTICLE INFO

Keywords:
Isolated mitochondria
Complex I deficiency
Complex III deficiency
Oxygen consumption
Coenzyme Q redox state
Reactive oxygen species

ABSTRACT

Mitochondrial disorders are hallmarked by the dysfunction of oxidative phosphorylation (OXPHOS) yet are highly heterogeneous at the clinical and genetic levels. Striking tissue-specific pathological manifestations are a poorly understood feature of these conditions, even if the disease-causing genes are ubiquitously expressed. To investigate the functional basis of this phenomenon, we analyzed several OXPHOS-related bioenergetic parameters, including oxygen consumption rates, electron transfer system (ETS)-related coenzyme Q (mtCoQ) redox state and production of reactive oxygen species (ROS) in mouse brain and liver mitochondria fueled by different substrates. In addition, we determined how these functional parameters are affected by ETS impairment in a tissue-specific manner using pathologically relevant mouse models lacking either *Ndufs4* or *Ttc19*, leading to Complex I (CI) or Complex III (CIII) deficiency, respectively. Detailed OXPHOS analysis revealed striking differences between brain and liver mitochondria in the capacity of the different metabolic substrates to fuel the ETS, reduce the ETS-related mtCoQ, and to induce ROS production. In addition, ETS deficiency due to either CI or CIII dysfunction had a much greater impact on the intrinsic bioenergetic parameters of brain compared with liver mitochondria. These findings are discussed in terms of the still rather mysterious tissue-specific manifestations of mitochondrial disease.

1. Introduction

The core of the mitochondrial electron transport system (ETS) is composed of four multi-subunit protein complexes and two electron shuttling molecules, i.e., mitochondrial coenzyme Q (mtCoQ), and cytochrome *c*. Reducing equivalents derived from nutrients are transferred from NADH and $FADH_2$ to molecular oxygen via the ETS. This process is coupled to proton pumping across the mitochondrial inner membrane, thus generating an electrochemical potential difference (or protonmotive force, *pmF*), which drives ATP production at F_1F_o ATP synthase. Overall, this whole process is termed oxidative phosphorylation (OXPHOS) [1]. Both Complex I (CI, NADH:ubiquinone oxidoreductase) and Complex II (CII, succinate dehydrogenase) reduce the ETS-reactive CoQ ($mtCoQ_{ox}$) to $mtCoQ_{red}$. In addition to CI and CII, other dehydrogenases such as the dihydroorotate dehydrogenase, electron transfer flavoprotein (ETF) or α-glycerophosphate dehydrogenase are able to reduce the mtCoQ. Therefore, it is evident that key metabolic pathways converge at the 'Q-junction' [2–4]. Downstream, Complex III (CIII, cytochrome bc_1 complex) then re-oxidizes $mtCoQ_{red}$ via the Q-cycle delivering reducing equivalents to cytochrome *c* [1]. Finally, Complex IV (CIV, Cytochrome *c* oxidase) oxidizes cytochrome *c*, reducing molecular oxygen to water.

* Correspondence to: A. L. Moore, School of Life Sciences, University of Sussex, Falmer, Brighton BN19QG, UK.
** Corresponding authors at: Department of Biomedical Sciences, University of Padova, Via Ugo Bassi 58/B, 35131 Padova, Italy.
E-mail addresses: a.l.moore@sussex.ac.uk (A.L. Moore), erika.fernandezvizarra@unipd.it (E. Fernandez-Vizarra), carlo.viscomi@unipd.it (C. Viscomi).
[1] These authors equally contributed.

https://doi.org/10.1016/j.bbadis.2024.167033
Received 27 May 2023; Received in revised form 15 December 2023; Accepted 16 January 2024

Mitochondrial diseases are a large family of highly heterogeneous disorders genetically determined by mutations in OXPHOS-related genes in either the nuclear genome or the mitochondrial DNA (mtDNA) [5]. Due to the polyploid nature of mtDNA, the variability in the clinical and biochemical outcomes in the mtDNA-related diseases was traditionally explained by the level of heteroplasmy, i.e., the proportion of mutated mtDNA molecules vs. wild-type (WT) molecules present in one cell. As mtDNA is randomly segregated in the daughter cells during mitosis, some cells may end up having higher loads of mutant mtDNA, thus exceeding the threshold necessary for impacting the function of the ETS [6]. However, many mitochondrial syndromes caused by pathological variants in nuclear housekeeping genes are still often present with tissue-specific manifestations. Similarly, also homoplasmic mutations in mtDNA often manifest with tissue-specific syndromes. The reasons for the diverse clinical presentations in these cases remain poorly understood and represent one of the key unsolved questions in the field [7]. In principle, it is usually accepted that tissues and cell types with higher energy requirements, such as neurons, cardiomyocytes and myocytes, are more susceptible to OXPHOS deficiency and that is why most of mitochondrial diseases manifest as neuromuscular disorders [8]. However, ETS is essential for almost every cell and tissue, and it is therefore unclear why some cells are more affected than others by OXPHOS defects. For instance, Leber's hereditary optic neuropathy (LHON), a prototypical mitochondrial disorder mainly due to homoplasmic mutations in *MT-ND4*, *MT-ND6* or *MT-ND1*, is characterized by the specific degeneration of the retinal ganglion cells [9]. Additional examples are mutations in several mitochondrial aminoacyl-tRNA synthetases, which are associated with diseases affecting only some cell types [10]. Several hypotheses have been proposed to explain the tissue-specificity. For instance, it has been suggested to be related to the varied metabolic roles mitochondria play in different cell types [11–13] where they have not only distinct biogenetic and functional properties but also diverse ETS activities [14,15]. In addition, different tissues show variations in the amounts and stoichiometry of ETS components, a result often suggested to be a possible explanation for tissue-specific tolerance to OXPHOS dysfunction observed in mitochondrial diseases [16–18]. Emerging data suggest that mitochondria from different tissues are able to fuel the ETS differently. For example, respiration in liver mitochondria relies much more on CII than on CI activity, whereas in heart the main entry point of reducing equivalents into the ETS is CI [19]. Accordingly, CI deficiency has a minimal impact on mitochondrial function and metabolism in the mouse liver [20]. Recently, divergent mutation-specific transcriptional responses triggered by mtDNA pathological variants in different cell lineages during embryonic development have been proposed to contribute to tissue-specificity of disease manifestations [21]. However, many questions remain unanswered as to how the diverse performance of mitochondria from different cell types can influence tissue dysfunction and disease in primary mitochondrial disorders.

In order to thoroughly investigate the functional basis of the striking tissue-specificity in mitochondrial diseases, we have analyzed several bioenergetic parameters, including oxygen consumption rates, the redox state of the ETS-reactive mitochondrial Q-pool, and ROS production in mouse brain and liver mitochondria fueled by different substrates and respiratory control using targeted inhibitors. Furthermore, we have determined how these functional parameters are affected by ETS impairment in a tissue-specific manner using pathologically relevant mouse models lacking either *Ndufs4* or *Ttc19*.

Ndufs4 encodes for the 18 kDa accessory subunit of the CI peripheral arm, which is located between the NADH-binding N-module and the Q-binding module [22–24]. Lack of Ndufs4 produces a particular assembly defect characterized by the destabilization and/or misincorporation of the N-module [25–27], maintaining a partial respiratory activity through CI [28]. In humans, pathological variants in *NDUFS4* cause Leigh syndrome (LS) [29], a recessive autosomal disease, also known as subacute necrotizing encephalopathy. LS patients manifest an early-onset fatal neurodegeneration, characterized by symmetric lesions in the subcortical nuclei, such as the brain stem nuclei, the thalamus, and the striatum [30]. However, involvement of other organs can also be present. A mouse model lacking *Ndufs4* (*Ndufs4*$^{-/-}$) reproduces the main features of the human disease and is widely used to study the underlying pathogenetic mechanisms and to test potential therapies [28,31,32]. Notably, brain-specific deletion of *Ndufs4* in mice recapitulates most of the features of constitutive knockout, confirming that the basis of the disease is mainly neurological [33].

Tetratricopeptide repeat domain 19 (TTC19) encodes for a protein of 35 kDa that was firstly described as a CIII assembly factor as it was found lacking in a cohort of patients biochemically characterized by isolated CIII deficiency [34]. The detailed molecular characterization of a *Ttc19*$^{-/-}$ mouse model allowed to determine that TTC19 facilitates the removal of the N-terminal fragments derived from the processing of the catalytic Fe—S Rieske subunit (Uqcrfs1), being necessary to maintain CIII function and structural integrity [35,36]. In humans, loss-of-function pathological variants in *TTC19* are the cause of purely neurological syndromes involving either early-onset slowly-progressing or late-onset rapidly-progressive neurodegeneration, occasionally with spinocerebellar ataxia, developmental delay and regression in childhood followed by psychosis [37,38]. In the *Ttc19*$^{-/-}$ mice, even though the CIII deficiency was present in all the analyzed organs, the only tissue showing pathological involvement was the brain [35].

This study supports the conclusion that mitochondria from different tissues handle the ETS redox reactions in a distinct way. Moreover, deficiencies of CI and CIII have a larger impact on the bioenergetic parameters of brain mitochondria than those of liver.

2. Materials and methods

2.1. Animal models

Ndufs4$^{-/-}$, *Ttc19*$^{-/-}$ and wild-type (WT) male and female mice with a C57BL/6J background were maintained under regulatory conditions according to the Italian and European directives (authorization no. 474/2020-PR). The animals were maintained in controlled environmental conditions with cycles of 12 h light/12 h dark and they were fed with a standard food diet and water ad libitum. Animals were sacrificed by cervical dislocation at 30–45 days of age for the *Ndufs4*$^{-/-}$ and their WT littermates, and at 4–5 months of age for the *Ttc19*$^{-/-}$ and their WT littermates. The available biochemical and functional data stemming from the thorough characterization of both mouse models, indicate that the sex variable has no influence in mitochondrial function in and the extent of the dysfunction in the mice [25,27,28,35]. Therefore, both male and female animals were used indistinctly in our analyses.

2.2. Mitochondrial isolation

Immediately after sacrifice, both brain and liver were quickly removed and placed in ice-cold PBS, and the mitochondria-enriched fractions for each tissue were promptly obtained as previously described [39]. Briefly, the tissues were minced into small pieces using scissors keeping the beaker in an ice bath. The tissue fragments were washed three times with ice-cold PBS and once with 5 ml of ice-cold IBc buffer (100 mM Tris-MOPS pH 7.4, 1 mM EGTA-Tris pH 7.4, 200 mM sucrose), resuspended in 3 ml of IBc buffer and transferred in a glass-Teflon potter to proceed with the homogenization with 10 strokes at 1600 rpm. The homogenized tissues were centrifuged at 600*g* for 10 min at 4 °C and the supernatants collected were centrifuged at 7000*g* for 10 min at 4 °C. The pellets collected were washed once in IBc buffer and centrifuged in the same conditions. The washed final pellet was resuspended in 300 μL of ice-cold mitochondrial respiration medium (MiR05; 0.5 mM EGTA, 3 mM $MgCl_2$, 60 mM Lactobionic acid, 20 mM Taurine, 10 mM KH_2PO_4, 20 mM HEPES adjusted to pH 7.1 with KOH at 30 °C, 110 mM D-sucrose, 1 g/L fatty acid-free BSA) [40]. The protein concentration of the enriched mitochondrial fractions was measured using

the DC protein assay (BioRad). In all experiments, 0.25 mg/ml of liver mitochondrial protein and 0.125 mg/ml of brain mitochondrial protein were used, in order to obtain similar O_2 fluxes per volume in the oxygraph chambers and to avoid reaching anoxia too early in the measurements of the brain samples.

2.3. High-resolution respirometry

Oxygen flux, mtCoQ redox state, and H_2O_2 flux of brain and liver mitochondria from both mouse models were measured using the NextGen-O2k (Oroboros Instruments, Innsbruck, Austria) and recorded using DatLab 7.4 and 8.0 (Oroboros Instruments) [41]. The O_2 signal was monitored by a polarographic oxygen sensor (POS) over time and the O_2 consumption of the mitochondria was plotted continuously. The polarographic oxygen sensor (POS) of the 2-ml O2k-chambers were calibrated daily (air calibration) at experimental temperature of 37 °C. Monthly instrumental O_2 background tests were performed including zero O_2 calibrations of the POS to correct for back diffusion into the chamber at low oxygen pressure. All experiments were performed in mitochondrial respiration medium MiR05.

2.4. Coenzyme Q redox measurement

The redox state of the ETS-reactive Q-pool in isolated mitochondria was assessed using a newly designed Q-Module incorporated in the NextGen-O2k [41]. The Q-Module consists of a three-electrode system and a mobile short chain mimetic CoQ_2. The CoQ_2 reacts with both the biochemical sites of the ETS and the measuring electrode. Cells contain non-mitochondrial and mitochondrial CoQ pools, and the total mitochondrial CoQ pools are partitioned into reactive and non-reactive CoQ (https://wiki.oroboros.at/index.php/Q-pools) [41]. Therefore, in the measurements performed in the described manner, the redox state of the CoQ_2 reflects the redox state of the ETS-reactive CoQ-pool.

The Q-sensor was calibrated as described to determine the oxidation and reduction peak potentials of CoQ_2 through cyclic voltammetry [41]. The O_2 flux and the redox state of the ETS-reactive CoQ were monitored simultaneously using a substrate-uncoupler-inhibitor-titration (SUIT) protocol (https://suitbrowser.oroboros.at/).

Briefly, the SUIT protocol consisted of adding 1 μM CoQ_2 to the chambers and following signal stabilization, 5 mM pyruvate and 2 mM malate were added to induce NAD^+-linked LEAK respiration (N-pathway). OXPHOS capacity was measured with a saturating concentration of ADP (2.5 mM), followed by 10 mM succinate which shows the additive effect of the S-pathway in the Q-junction. Respiration linked to CI was blocked with 0.5 μM rotenone and the electron transfer capacity was assessed by titration with the uncoupler carbonyl cyanide 4-(trifluoromethoxy)phenylhydrazone (FCCP) (0.5 μM/step) followed by the induction of anoxia. To determine the CoQ redox state in the same respiratory states employed to evaluate ROS production, we induced RET with 10 mM succinate, then, OXPHOS capacity was supported with 2.5 mM ADP. After, 5 mM pyruvate was added to induce NADH pathway, and rotenone (0.5 μM) was added to inhibit CI. The protocol was ended with the induction of anoxia. In both protocols, the fraction of $mtCoQ_{red}$ was calculated determining the CoQ_2 electrical current signal using the DatLab 7.4 software, and setting as 0 the value of the CoQ_2 signal corresponding to the fully oxidized mtCoQ, i.e., before adding any substrate, and the value of 1 to the signal corresponding to the fully reduced CoQ_2 in anoxia (see ref. [41]).

2.5. ROS production

H_2O_2 flux was measured simultaneously to respiration with the NextGen-O2k including the O2k-Fluo Smart Module in MiR05. Extramitochondrial H_2O_2 production was measured using 10 μM Amplex UltraRed® (AmR) in the presence of 1 U/ml horseradish peroxidase (HRP) and 5 U/ml superoxide dismutase (SOD). The fluorescent product Amplex UltraRed was continuously monitored [42]. The fluorescence intensity was calibrated with repeated titrations of 0.1 μM fresh H_2O_2. Multiple H_2O_2 calibrations were performed during the experiment to measure the changes in the sensitivity (V/μM) towards H_2O_2 over time [43]. The fluorescence slope was calculated as the non-linear time derivate of the fluorescence signal using DatLab 7.4. To study the H_2O_2 flux induced by reverse electron transport (RET) in the liver and brain mitochondria, we used a different SUIT protocol (SUIT-009) (https://suitbrowser.oroboros.at/). In order to inhibit the interferences of internal carboxylesterases in the fluorescence signal during the Amplex UltraRed assay [44], we added 250 μM of phenylmethylsulfonyl fluoride (PMSF) before inducing the LEAK state with 10 mM succinate to support RET [45]. OXPHOS capacity was induced by 2.5 mM ADP and NADH-pathway was induced with 5 mM pyruvate. Inhibition of CI was achieved by the addition of 0.5 μM rotenone and finally, respiration was fully inhibited by the addition of 2.5 μM Antimycin A.

2.6. Mitochondria membrane potential

Mitochondrial membrane potential of liver mitochondria was measured using the fluorescent probe safranin *O* and the O2k-Fluo Smart module. Once the baseline was recorded, the fluorescent signal was calibrated by fourth consecutive additions of 0.5 μM safranin *O* until reaching a concentration of 2 μM. Then, the mitochondrial-enrichment fraction was injected into the chambers inducing the uptake of the dye. The mt-MP in each respiratory state was evaluated. The NADH-pathway was engaged with 5 mM pyruvate and CI was inhibited with rotenone (0.5 μM). Respiration was fully inhibited by anoxic conditions. Changes in the safranin fluorescent signal were continuously monitored throughout the experiment. The calibrated fluorescence signal (μM) was used to determine ΔΔpsi in each respiratory state, using the values obtained in anoxia as the measure of the minimum membrane potential (Δpsi), which was set to 1.

2.7. Data analysis

For all traces, only the steady state of oxygen flux, $mtCoQ_{red}$ and H_2O_2 flux were selected, excluding unavoidable titration artefacts by chemical additions or intermittent re-oxygenations of the incubation medium. The respiratory steady states marked in each experiment were compared with *t*-test or two-way ANOVA with Sidak's multiple comparisons test using GraphPad Prism 8.0.

2.8. Chemicals

Amplex UltraRed® was obtained from Life Technologies. H_2O_2, HRP, SOD, CoQ_2 and safranine *O* substrates, inhibitors and the components of MiR05 were purchased from Sigma-Aldrich. DC Protein Assay was from Bio-Rad.

3. Results

3.1. Tissue- and age-specific bioenergetic features in brain and liver mitochondria

To obtain a detailed insight into the tissue-specific differences of bioenergetic parameters in WT tissues, we first investigated oxygen consumption in different pathway- and coupling-control states in mitochondria isolated from brain and liver of young (i.e.: 30–45 days old) and adult (i.e.: 4–5 months old) WT mice. Changes in the ETS-reactive CoQ redox state and O_2 consumption were determined simultaneously (Fig. 1 and Suppl. Figs. S1 and S3).

The N-pathway, i.e. through the oxidation of NADH at the level of CI, was stimulated by the addition of pyruvate and malate (PM) to the O2k-chambers. The non-phosphorylating respiratory rate (LEAK respiration) was low and similar in both tissues at both ages (Fig. 1A and B, Suppl.

Figs. S1 and S3A and B). PM increased $mtCoQ_{red}/mtCoQ_{tot}$ (X_{Qred}) to ~0.3 in both brain and liver mitochondria isolated from young animals (Fig. 1C, Suppl. Figs. S1A, C, S3C and D). In contrast, $mtCoQ_{red}/mtCoQ_{tot}$ in this state was ~0.8 in liver mitochondria from adult mice (Fig. 1D and Suppl. Figs. S1B and S3C), whilst it remained low (~0.2) in adult brain mitochondria. The addition of ADP (D) transitioned the mitochondria into the phosphorylating (OXPHOS) state, increasing oxygen consumption in mitochondria from both tissues (Suppl. Fig. S1). However, even though the O_2 fluxes might be somewhat underestimated due to the presence synaptosomes in the brain preparations, containing mitochondria that are inaccessible to the added substrates [46], NAD^+-linked respiration in the OXPHOS state was substantially higher in brain than in liver mitochondria at both ages (~600 vs ~200 pmol·s^{-1}·mg prot^{-1}) (Fig. 1A and B). The increase in downstream electron fluxes in OXPHOS resulted in CoQ_2 oxidation, leading to a $mtCoQ_{red}/mtCoQ_{tot}$ ratio of 0.1–0.15. This value was higher (0.3) in liver mitochondria from the adult mice (Fig. 1C and D and Suppl. Figs. S1B, D and S3C). Succinate, which supplies additional electrons at the level of CII, caused an increase in oxygen consumption via the convergent NS-pathway in mitochondria from both tissues and age groups (Fig. 1A and B, Suppl. Fig. S3A and B). N/NS and S/NS ratios are indexes of how much N- and S- pathways, respectively, contribute to the overall electronic flux. Young liver mitochondria showed N/NS ratio of ~0.2, which was significantly lower than those of the brain mitochondria, (~0.5–0.6) (Fig. 1E). This is compatible with the fact that the addition of succinate stimulated respiration of liver mitochondria from young mice much more than those from the older group (900 vs 450 pmol·s^{-1}·mg^{-1}) (Suppl. Fig. S3A). Interestingly, the N/NS ratios in liver mitochondria from adult mice were higher and much more similar to those of brain mitochondria (Fig. 1F), which remained unchanged with age (Suppl. Fig. S3F). Under the convergent NS-pathway conditions, $mtCoQ_{red}/mtCoQ_{tot}$ increased to approximately 0.3 in brain, comparable to what previously reported in heart mitochondria [47], whilst it increased to 0.9–1.0 in liver (Fig. 1C and D). Rotenone decreased oxygen consumption to pre-succinate levels in brain but had no effect on the respiratory rates in liver mitochondria (Fig. 1A and B, Suppl. Fig. S3A and B). Accordingly, the S/NS ratio was ~0.6 in brain mitochondria (Fig. 1E, F, Suppl. Fig. S3F), whereas it was ~1.0 in the samples from the young mice and ~0.8 in the adult ones (Fig. 1E and F, Suppl. Fig. 3E). These data indicate that liver preferentially relies on the S-pathway in the presence of both NADH-linked (CI) substrates and succinate (CII), as previously proposed [19]. In contrast, in brain mitochondria the N/NS- and S/NS-ratios were ~0.6 and ~0.7, respectively, indicating a certain degree of additivity [48], similarly to heart mitochondria [19,41,47].

The uncoupler (U) FCCP stimulated succinate-driven respiration only in liver mitochondria from the adult animals (Fig. 1A and B, Suppl. Figs. S1A, S3A and B), indicating that OXPHOS capacity of brain mitochondria at all ages and of liver mitochondria from young animals is not limited by the capacity of the phosphorylation system, i.e., the capacities of generating and utilizing the *pmF* are matched. Furthermore, uncoupling had no significant effect on the mtCoQ redox state in both types of mitochondria, which remained highly reduced in liver compared with brain (Fig. 1C and D, Suppl. Fig. S3C and D). Anoxia (Anox) conditions completely reduce the mtCoQ pool, and were used as the measure of fully reduced mtCoQ pool ($mtCoQ_{red}/mtCoQ_{tot} = 1$). Such data indicate that brain and liver have different intrinsic substrate usage or respiratory pathway preferences. In addition, they indicate that mitochondrial function and spare respiratory capacity are age dependent in liver but not in brain mitochondria.

We next analyzed oxygen consumption rates simultaneously with reactive oxygen species (ROS) production when feeding the mitochondria with a different combination of substrates and inhibitors (Suppl. Fig. S2) using Amplex UltraRed to detect H_2O_2. In addition, we carried out these experiments in the presence of the carboxylesterase inhibitor PMSF, which is necessary to avoid the interference of these enzymes, especially in the liver mitochondria where their activity is particularly high [44]. ROS production was induced by feeding the ETS with succinate (S) in wild-type mitochondria from both tissues at both ages. In the absence of rotenone and ADP, this condition triggers ROS production via reverse electron transfer (RET) at the level of CI when the membrane potential is high and the ETS-reactive CoQ pool is largely reduced [49,50]. Accordingly, succinate addition (S) increased the reduced mtCoQ fraction and the membrane potential (Suppl. Fig. S4) and produced an increase in ROS production in wild-type mitochondria from both tissues at both ages, being significantly higher in the brain compared with the liver mitochondria (Fig. 2C and D) and in the young animals compared with the adults (Suppl. Fig. S5C and D). ADP stimulated the O_2 flux (Fig. 2A and B and Suppl. Figs. S4C, D, S5A and B) and markedly decreased H_2O_2 production (Fig. 2C and D and Suppl. Fig. S5C and D) in brain and liver mitochondria, undoubtedly due to re-oxidation of the mtCoQ-pool and diminution of the membrane potential (Suppl. Fig. S4C and D), thereby inhibiting RET. Pyruvate addition did not affect oxygen consumption in either tissue (Fig. 2A and B), and did not affect ROS being production in the presence of NADH-linked substrates such as pyruvate (P) (Fig. 2C and D). The subsequent addition of rotenone induced higher H_2O_2 production only in brain mitochondria, being more prominent in the organelles from the young mice (Fig. 2C and D, Suppl. Fig. S5C and D). Whilst rotenone inhibits ROS generation in RET conditions, when there is forward electron transfer (FET), rotenone can increase ROS production [51]. Notably, the addition of rotenone did not decrease respiration under these conditions, consistent with the results shown in Fig. 1A and B, whilst antimycin A completely blocked oxygen consumption, and maintained higher ROS production in the mitochondria from young brains (Fig. 2C and D, Suppl. Fig. S5C and D).

Altogether, these results suggest that the origin and regulation of ROS production at the level of Complex I differ between brain and in liver mitochondria and that the age of the animal also has an influence on this phenomenon.

3.2. *Effects of Complex I deficiency on bioenergetic parameters in brain and liver mitochondria*

To elucidate how CI deficiency affected the bioenergetic parameters in liver and brain mitochondria, we analyzed O_2 fluxes, ETS-reactive CoQ redox state and ROS production in samples from young *Ndufs4*$^{-/-}$ and WT mice. We used the young animals because the *Ndufs4*$^{-/-}$ mice do not survive beyond 55 days [28].

In liver mitochondria, no differences between WT and *Ndufs4*$^{-/-}$ were observed in the oxygen consumption rate with either NADH or succinate-linked substrates in non-OXPHOS conditions (Fig. 3A). As previously observed in WT mitochondria (Fig. 1A and B), respiration in presence of PM and ADP was much lower than that observed following the addition of succinate (Fig. 3A), again supporting the idea that succinate is the main source of reducing equivalents for liver mitochondria. Accordingly, the N/NS ratio was 0.2–0.3 in the WT and *Ndufs4*$^{-/-}$ liver mitochondria, whereas the S/NS ratio was close to 1 in both groups (Fig. 3E). No difference was observed on the reduced mtCoQ fraction under any condition (Fig. 3C). Altogether, these observations indicate that CI deficiency, induced by the loss of the NDUFS4 subunit, does not impact liver mitochondrial bioenergetic properties, similar to that found in an *Ndufa9* KO mouse model [20].

In contrast, O_2 consumption rates were significantly decreased in the *Ndufs4*$^{-/-}$ brain mitochondria respiring on CI-linked substrates (PM) and in the presence of ADP (D), compatible with a CI defect (Fig. 3B). Accordingly, N/NS ratios were decreased to about half of the control (~0.3 vs. ~0.6) (Fig. 3F). Moreover, N-pathway substrates reduced mtCoQ to a lesser extent in *Ndufs4*$^{-/-}$ vs WT brain mitochondria. This difference was significant in the LEAK state (Fig. 3D). No statistically significant differences between the two genotypes were observed following the addition of succinate and rotenone (Fig. 3B), although the S/NS ratio was somewhat increased in the *Ndufs4*$^{-/-}$ brain mitochondria (Fig. 3F). Differences in the CoQ_2 redox state in *Ndufs4*$^{-/-}$ brain

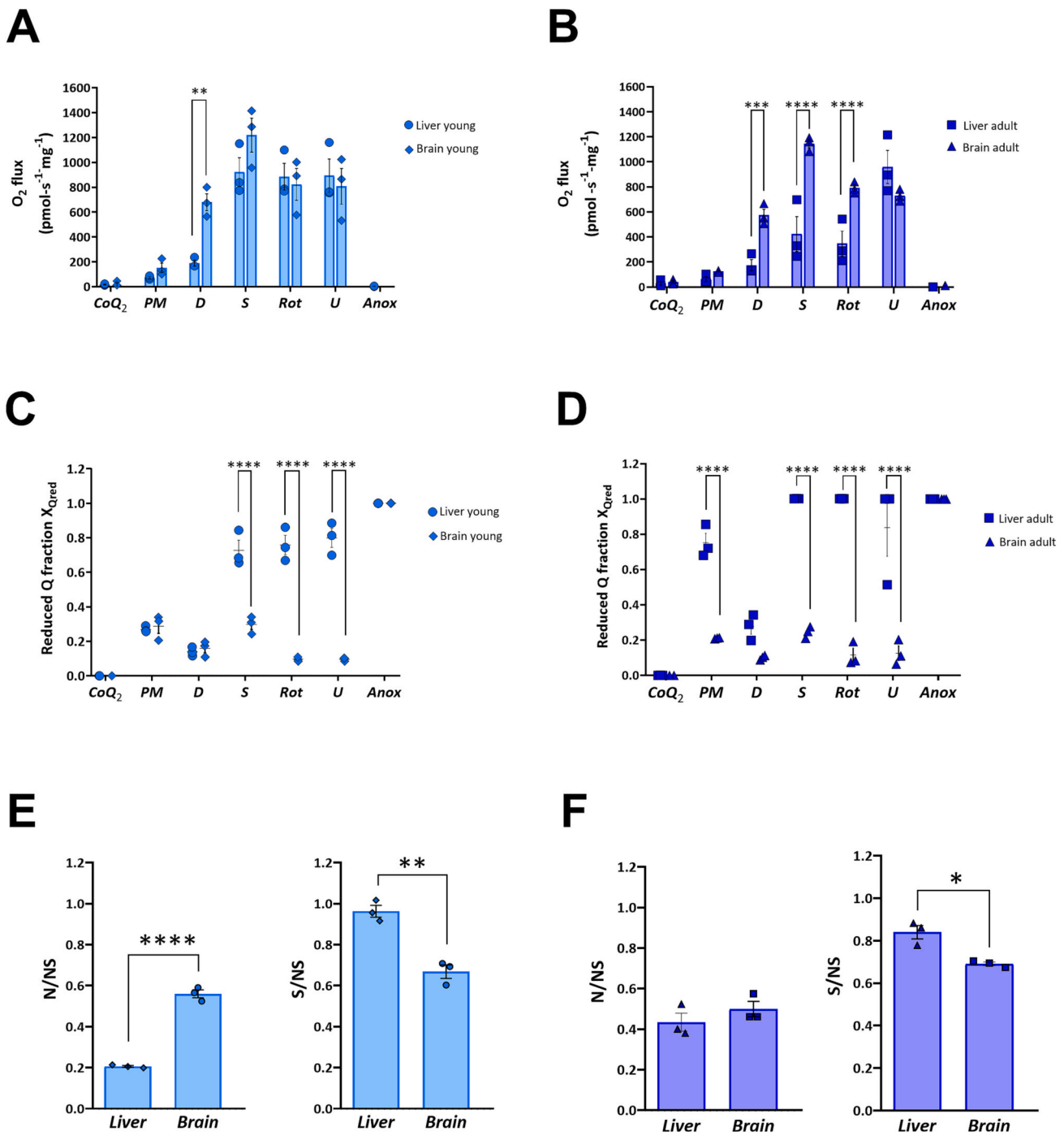

Fig. 1. Mitochondrial respiration and CoQ_2 redox state in isolated mitochondria are tissue and age-specific. (A) Protein mass-specific O_2 flux of liver and brain mitochondria from 30 to 45-day-old WT mice. (B) Protein mass-specific O_2 flux of liver and brain mitochondria from 4 to 5-month-old WT mice. (C) Reduced Q fraction (X_{Qred}) measured simultaneously with O_2 fluxes in the samples shown in panel (A). (D) X_{Qred} measured simultaneously with O_2 fluxes in the samples shown in panel (B). Respiration in isolated mitochondria were fueled by sequential addition of different respiratory substrates: NAD-linked substrates (N- or CI-linked) pyruvate and malate (PM) to induce non-phosphorylating (LEAK) respiration; ADP (D) to induce N-linked respiration coupled to ATP synthesis (OXPHOS capacity) and succinate (S) to induce S-linked (or CII-linked) respiration, providing the additive effect of donating electrons to the Q-junction from both CI and CII. CI was blocked with rotenone (Rot) and afterwards, the uncoupler CCCP (U) was added to induce maximum electron transfer (ET) capacity. Oxygen was depleted in the measuring chamber, inducing anoxia (Anox), a situation in which the ETS-reactive Q-pool is completely reduced and it was used to calibrate the raw Q-signal, setting the $X_{Qred} = 1$. (E) N/NS and S/NS pathway control ratios calculated for liver and brain mitochondria from young WT mice. (F) N/NS and S/NS pathway control ratios calculated for liver and brain mitochondria from adult WT mice. The N/NS ratios were calculated by dividing the oxygen consumption rates from the N-Pathway (PM + D) by the oxygen consumption rates from the NS-convergent pathway (PM + D + S). The S/NS ratios were calculated by dividing the oxygen consumption rates from the S-Pathway (PM + D + S + Rot) by the oxygen consumption rates from the NS-convergent pathway (PM + D + S). The data in the graphs are presented as the mean ± SD of three independent experiments ($n = 3$). Statistically significant differences were determined using two-way ANOVA with Sidak's multiple comparisons test and unpaired *t*-test (*$p < 0.05$; **$p < 0.01$; ****$p < 0.0001$).

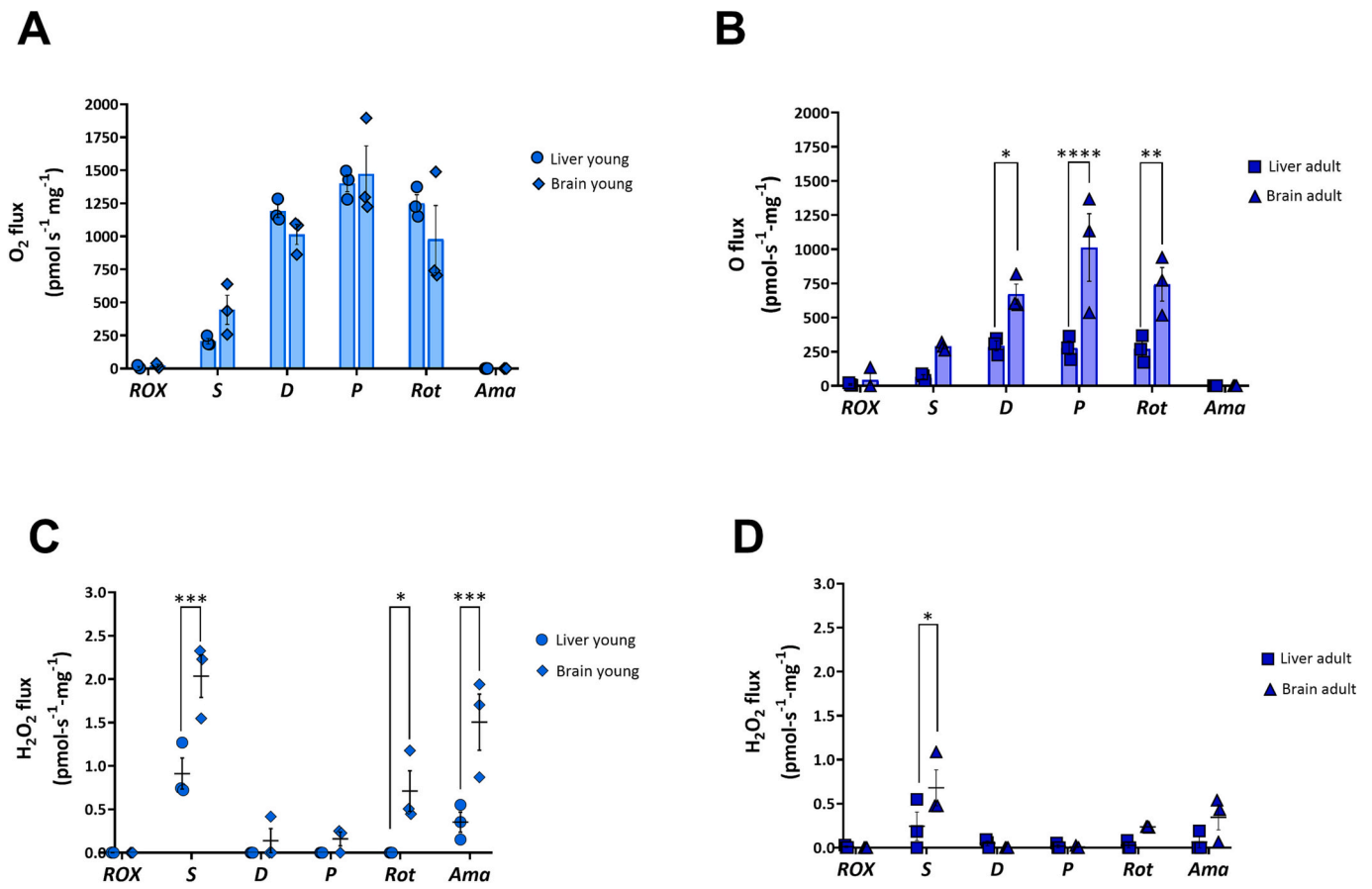

Fig. 2. ROS production measured in isolated mitochondria depends on the tissue of origin. (A) Specific O_2 flux in liver and brain mitochondria from young WT mice. (B) Specific O_2 flux of liver and brain mitochondria from adult WT mice. (C) Mass-specific H_2O_2 flux in the samples shown in panel (A). (D) Mass-specific H_2O_2 flux in the samples shown in panel (B). Oxygen consumption and H_2O_2 production were measured in the presence of mitochondria without adding any substrates (MITO). Reverse electron transfer (RET) was induced by addition of succinate (S) in the absence of ADP. Thereafter ADP (D) was added to induce S-linked OXPHOS capacity. Pyruvate (P) was added to fuel CI (NADH)-linked respiration, and rotenone (Rot) was then added to block it. Antimycin A (Ama) was added to inhibit CIII. The data in the graphs are presented as the mean ± SD of three or four independent experiments ($n = 3$ or 4). Statistically significant differences were determined using two-way ANOVA with Sidak's multiple comparisons test (*$p < 0.05$; **$p < 0.01$; ***$p < 0.001$; ****$p < 0.0001$).

mitochondria were also observed in the presence of succinate (Fig. 3D). This result suggests that in brain mitochondria CI deficiency has a major impact on the redox state of the ETS-reactive CoQ-pool in the *Ndufs4*$^{-/-}$ mice, not only in the presence of PM but also when electrons are being fed through CII. Interestingly, succinate, which increased oxygen consumption by approximately 2-fold, did not reduce CoQ_2 over the levels achieved with PM in neither genotype and rotenone decreased the reduced mtCoQ fraction to similar levels in WT and KO.

We also analyzed oxygen consumption and ROS production in *Ndufs4*$^{-/-}$ liver and brain mitochondria in comparison with the corresponding WT controls, using the SUIT protocol for the evaluation of ROS production (see Materials and methods). No significant differences were found in the respiratory rates between the WT and the CI-deficient mitochondria (Fig. 4A and B). ROS production in RET conditions, was slightly but significantly higher in liver mitochondria from the *Ndufs4*$^{-/-}$ mice (Fig. 4C), whilst in brain mitochondria the addition of only succinate induced significantly lower ROS production in *Ndufs4*$^{-/-}$ vs. WT (Fig. 4D). However, in WT brain mitochondria succinate-induced ROS production was decreased by ADP addition to the same levels shown in the *Ndufs4*$^{-/-}$ brains, indicating a larger involvement of CI and RET in ROS production in brain mitochondria in comparison with liver.

3.3. Effects of Complex III deficiency on bioenergetic parameters in brain and liver mitochondria

For this set of experiments, we used adult animals because *Ttc19*$^{-/-}$ mice have a normal lifespan [35]. In liver mitochondria from *Ttc19*$^{-/-}$ mice, oxygen consumption rates and, consequently the N/NS and S/NS ratios, were basically the same to WT under different pathway and coupling control states, the only significant difference being the maximum electron transfer (ET) capacity in the presence of an uncoupler (U) (Fig. 5A and E). Even though the $mtCoQ_{red}/mtCoQ_{tot}$ ratio was lower in the *Ttc19*$^{-/-}$ in comparison to WT in the N-linked pathway LEAK state, the addition of succinate after ADP, was able to completely reduce the ETS-reactive CoQ pool in both WT and KO liver mitochondria (Fig. 5C).

In contrast, oxygen consumption was markedly reduced in brain mitochondria from *Ttc19*$^{-/-}$ mice in the presence of succinate and in the uncoupler-induced ET state (Fig. 5B). This is in agreement with a partial deficiency in the oxidation capacity downstream of the Q-junction, impeding electron flow to the terminal oxidases at maximum capacity. Accordingly, CoQ_2 was significantly reduced in *Ttc19*$^{-/-}$ compared to WT brain mitochondria under all conditions (Fig. 5B and D). Both N/NS and S/NS ratios were significantly increased in brain *Ttc19*$^{-/-}$ brain mitochondria (Fig. 5F), due to the significant reduction of the NS-pathway rates in these samples (Fig. 5B).

O_2 consumption (Fig. 6B and A) and ROS production via RET were

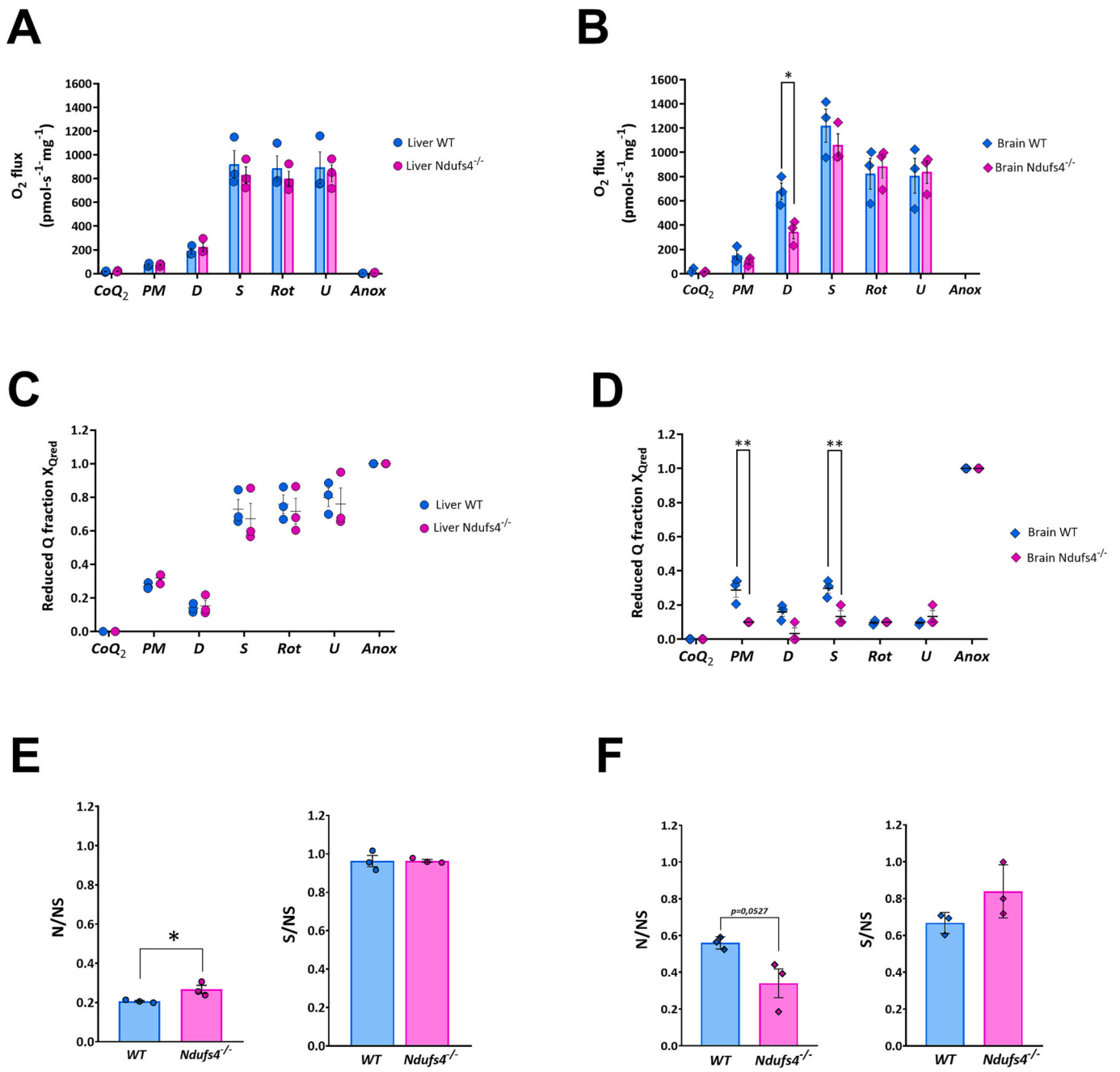

Fig. 3. Mitochondrial respiration and ETS-reactive CoQ redox state are affected in brain mitochondria from mice with CI deficiency. (A) Specific O_2 flux in liver mitochondria from WT and Ndufs4$^{-/-}$ mice. (B) Specific O_2 flux in brain mitochondria from wild-type (WT) and Ndufs4$^{-/-}$ mice. (C) X_{Qred} in the samples shown in panel (A). (D) X_{Qred} in the samples shown in panel (B). The different respiratory states were induced as described in Fig. 1. (E) N/NS and S/NS pathway control ratios calculated for liver mitochondria from young WT and Ndufs4$^{-/-}$ mice. (F) N/NS and S/NS pathway control ratios calculated for brain mitochondria from young WT and Ndufs4$^{-/-}$ mice. The ratios were calculated as described in Fig. 1. The WT mice were the same used in Figs. 1 and 2 in the "young" group. The data in the graphs are presented as the mean ± SD of three independent experiments ($n = 3$). Statistically significant differences were determined using two-way ANOVA with Sidak's multiple comparisons test ($^*p < 0.05$; $^{**}p < 0.01$).

similar in *Ttc19*$^{-/-}$ vs WT liver mitochondria, but *Ttc19*$^{-/-}$ brain mitochondria generated less ROS than the WT in these conditions (Fig. 6C and D). Furthermore, no difference between the two genotypes was observed following the addition of ADP, the NADH-linked substrate pyruvate (P) or the CI and CIII inhibitors, in both liver and brain mitochondria.

4. Discussion

In this work, we investigated the tissue-specific bioenergetic features in brain and liver of wild-type mice and pathologically relevant mouse models. We discovered that brain and liver mitochondria utilize different metabolic substrates to drive respiration. In particular, we found that brain mitochondria can efficiently use both CI-linked substrates and succinate to sustain respiration, whilst liver mitochondria mostly rely on CII activity. Similar findings have been recently reported in the literature showing a higher dependence for CII-linked respiration in liver than in heart mitochondria, reflecting the higher relative abundance of CII over CI in the liver [19,20,50]. In addition, the regulation of the relative contribution of CI-linked vs. CII-linked pathways in

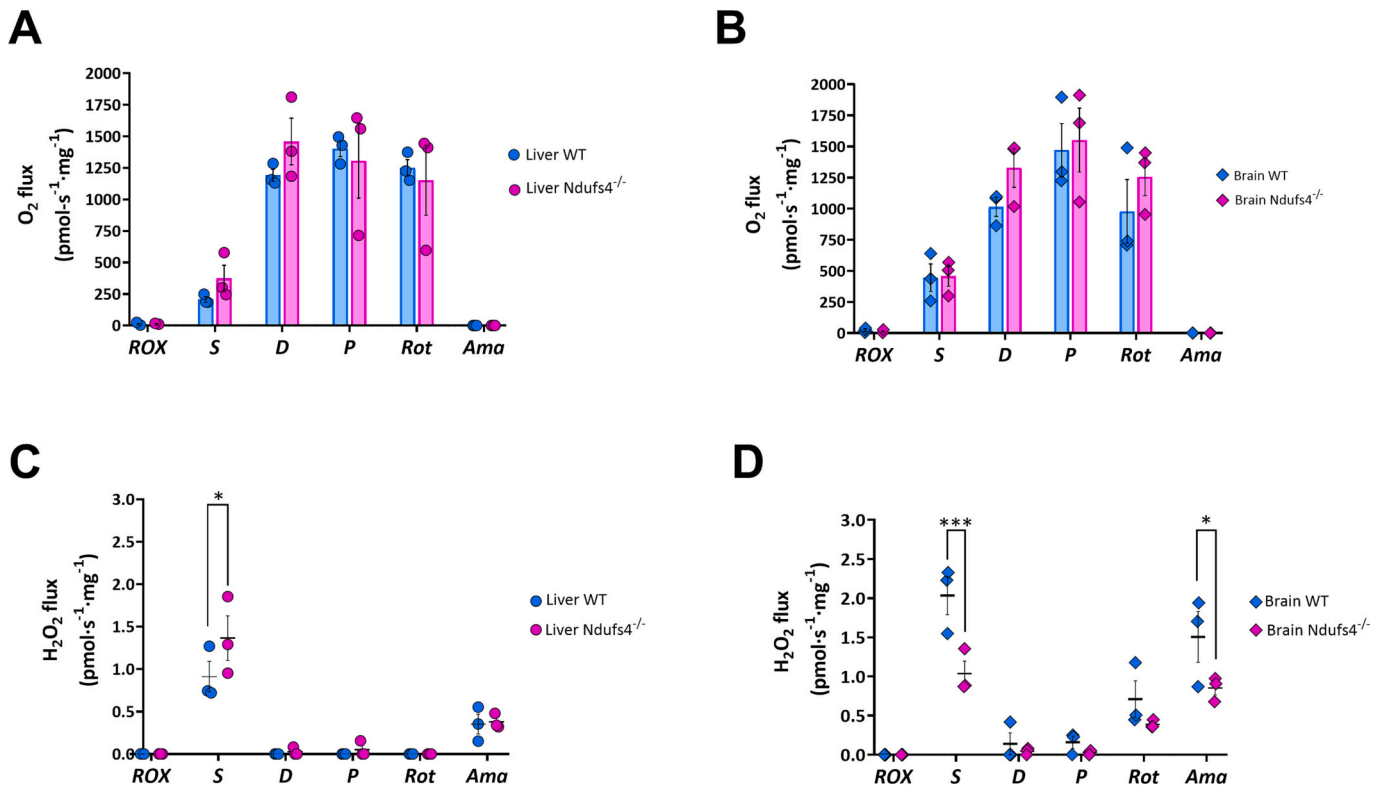

Fig. 4. ROS production is altered in brain and liver mitochondria from mice with CI deficiency. (A) Specific O_2 flux in liver mitochondria from WT and Ndufs4$^{-/-}$ mice. (B) Specific O_2 flux in brain mitochondria from WT and Ndufs4$^{-/-}$ mice. (C) Specific H_2O_2 flux of the samples shown in panel (A). (D) Specific H_2O_2 flux measured in parallel to the samples in panel (B). The different respiratory states were induced as described in Fig. 2. The data in the graphs are presented as the mean ± SD of three or four independent experiments (n = 3 or 4). The WT mice were the same used in Figs. 1 and 2 in the "young" group. Statistically significant differences were determined using two-way ANOVA with Sidak's multiple comparisons test (*$p < 0.05$; ***$p < 0.001$).

different metabolic states occurs via a mechanism involving CII inhibition by oxalacetate [19]. CII is not the only mitochondrial dehydrogenase, other than CI, that can reduce the mtCoQ pool. In fact, there are several metabolic routes that converge into CoQ as the final electron acceptor, feeding the reducing equivalents to the terminal part of the ETS [2]. In our experiments we have used succinate as the only $FADH_2$-linked electron donor, allowing us to test the relative contribution of CI vs. CII to the observed respiratory activity in the two analyzed tissues, whilst the interplay between the CI pathway (NADH-linked) and all the other $FADH_2$-linked pathways working simultaneously in the mitochondria of different tissues in vivo, remains to be established. One of the most important aspects of our analysis is that we were able to assess the redox state of the ETS-reactive CoQ-pool simultaneously with oxygen consumption using different substrates under varying coupling and pathway respiratory states [41,52]. We found that respiration, stimulated by different substrates, and the corresponding mtCoQ redox state had striking tissue-specific differences. Simultaneously monitoring the redox state of the Q-pool using the Q-module electrode-based method, revealed that the mtCoQ pool is much more reduced in lever compared with brain in all the respiratory states. Tissue-specific differences in the CoQ redox poise were previously found by measuring the total CoQ content in respiring mitochondria by HPLC [18]. Continuously monitoring steady-state changes in the redox state of the Q-pool turned out to be extremely informative. In particular, we found that in brain the $mtCoQ_{red}$ fraction is only partially increased by succinate, whilst in liver mitochondria mtCoQ is fully reduced under the same conditions. This latter result fits with previous data showing that succinate oxidation fully reduces the Q-pool both under non-phosphorylating and phosphorylating conditions [50,53,54]. Such findings suggest that in each tissue, the ETS has different intrinsic properties. This could be due to different stoichiometries of the ETS elements in different cell types [18] or to other variations in mitochondrial function, metabolism and/or respiratory control [11,15–17]. Accordingly, our data clearly indicate intrinsic metabolic divergence between brain and liver. Whether such metabolic differences can totally explain the tissue-specificity of mitochondrial function and dysfunction warrants further investigation. Recent evidence indicated that tissue specificity in mtDNA mutations can be related to cell lineage-specific transcriptional networks which are established early during embryonic development [21]. However, it is currently unknown if this is the case also for nuclear mutations.

Our work has also unraveled unanticipated tissue- and age-specific differences in ROS production via RET induced by succinate under non-phosphorylating conditions. In this way, brain mitochondria produced more ROS than liver mitochondria and the key role of CI in this phenomenon in brain is revealed by the lower H_2O_2 fluxes observed in the *Ndufs4*$^{-/-}$ brain mitochondria in comparison to the control. The low rate of ROS produced under the experimental conditions is partly unexpected, as ROS is usually considered as a major contributor to the pathogenesis of mitochondrial diseases via oxidative stress [55]. Our data suggest that the relationship between ETS dysfunction and increased ROS production is not direct and hence ROS itself is not a major cause of the disease phenotypes. In fact, ROS is emerging as an important signaling molecule regulating mitochondrial biogenesis [56] and, in some pathological circumstances, reducing ROS production worsens the clinical and biochemical phenotype of mitochondrial disease models [45].

Another important observation which arises from our data is that mice age has a significant influence on the bioenergetic capacities of liver mitochondria, with differences apparent in oxygen consumption rates in the LEAK state fueled by NADH-linked substrates, as well as in the ETS-reactive CoQ redox state. In contrast, in brain mitochondria from the two age groups, these parameters were the same. This

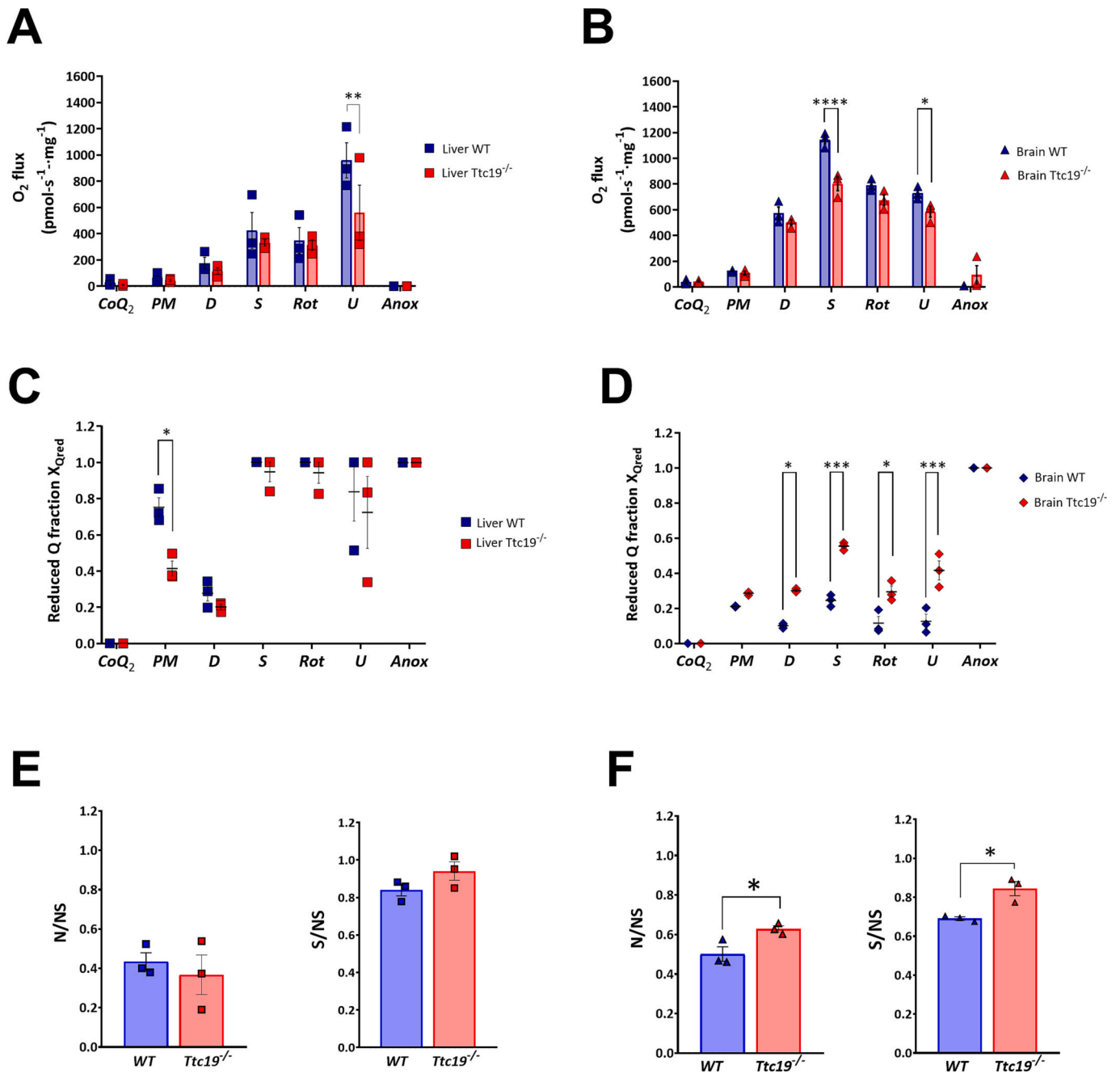

Fig. 5. Mitochondrial respiration and ETS-reactive Q redox state are affected in liver and brain mitochondria from mice with CIII deficiency. (A) Specific O_2 flux in liver mitochondria from wild-type (WT) and Ttc19$^{-/-}$ mice. (B) Specific O_2 flux in brain mitochondria from WT or Ttc19$^{-/-}$ mice. (C) X_{Qred} in the samples shown in panel (A). (D) X_{Qred} in the samples shown in panel (B). The different respiratory states were induced as described in Fig. 1. The data in the graphs are presented as the mean ± SD of three independent experiments ($n = 3$). (E) N/NS and S/NS pathway control ratios calculated for liver mitochondria from young WT and Ttc19$^{-/-}$ mice. (F) N/NS and S/NS pathway control ratios calculated for brain mitochondria from young WT and Ttc19$^{-/-}$ mice. The ratios were calculated as described in Fig. 1. The WT mice were the same used in Figs. 1 and 2 in the "adult" group. Statistically significant differences were determined using two-way ANOVA with Sidak's multiple comparisons test (*$p < 0.05$; **$p < 0.01$; ***$p < 0.001$; ****$p < 0.0001$).

observation could be explained by the fact that the brain is one of the first organs to develop and does not undergo size changes after the first two weeks of the mouse life, whereas liver growth and differentiation continues to occur until the second month [57]. Therefore, it is plausible that liver metabolism is different at one month and five months of age, whereas brain metabolism does not change during that period. Although ROS production was higher in brain than in liver mitochondria, organelles isolated the tissues of young mice generally produced more ROS in comparison with those from older mice.

We also analyzed mitochondria isolated from brain in liver from pathologically relevant mouse models. In particular, we used the phenotypically well characterized *Ndufs4*$^{-/-}$ [28,31,33] and *Ttc19*$^{-/-}$ [35] mice as models of CI and CIII deficiency, respectively. ETS defects had a much more noticeable impact on the bioenergetic parameters of brain than liver mitochondria, although the effects did depend on the origin of the deficiency. The oxygen consumption shown by the *Ndufs4*$^{-/-}$ brain mitochondria were compatible with a CI enzymatic defect, i.e. significantly lower rates were observed in the presence of CI-linked substrates in the OXPHOS state (PM + D). The differences shown in the reduced mtCoQ fractions, being decreased in the *Ndufs4*$^{-/-}$, are

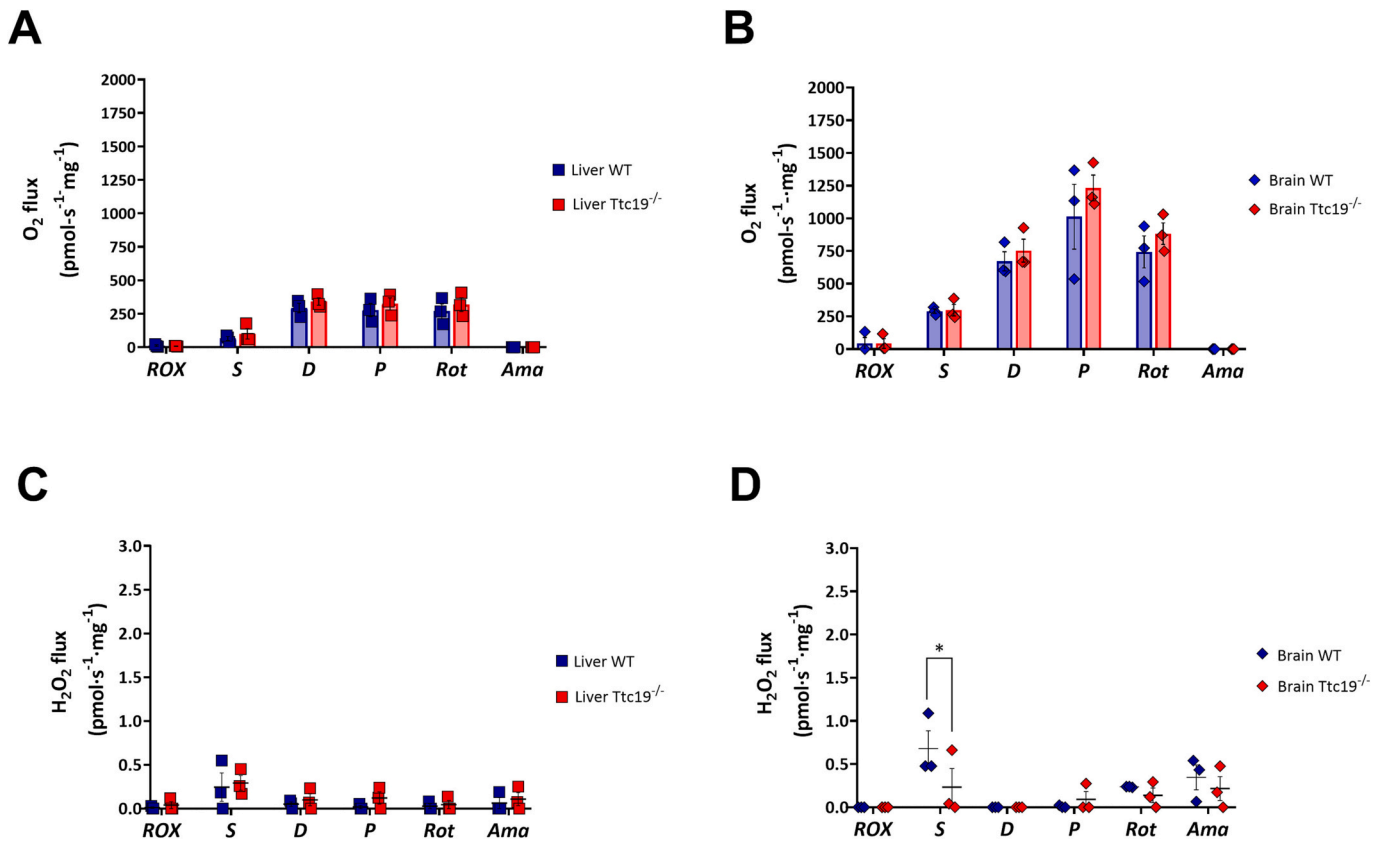

Fig. 6. ROS production remained unaltered in brain and liver mitochondria from mice with CIII deficiency. (A) Specific O_2 flux in liver mitochondria from WT or Ttc19$^{-/-}$ mice. (B) Specific O_2 flux in brain mitochondria from W or Ttc19$^{-/-}$ mice. (C) Specific H_2O_2 flux in the samples shown in panel (A). (D) Specific H_2O_2 flux in the samples shown in panel (B). The different respiratory states were induced as described in Fig. 2. The WT mice were the same used in Figs. 1 and 2 in the "adult" group. The data in the graphs are presented as the mean ± SD of three or four independent experiments (n = 3 or 4). Statistically significant differences were determined using two-way ANOVA with Sidak's multiple comparisons test (*$p < 0.05$).

also compatible with lower electron fluxes through the Q-junction originating from CI. However, none of these differences were observed in liver mitochondria, in agreement with the idea that CI deficiency has a minimal impact on mitochondrial function and metabolism in liver [20]. Conversely, CIII deficiency produced lower respiratory rates in brain mitochondria under phosphorylating conditions in the presence of combined CI + CII-linked substrates, i.e., compatible with a partial lower capacity for accepting reducing equivalents downstream of the Q-junction. This lower oxidizing capacity of the ETS-reactive Q-pool was also reflected in an increase in reduced mtCoQ fractions measured in the *Ttc19*$^{-/-}$ brain compared to WT mitochondria. Again, in liver mitochondria the impact on respiration and CoQ_2 redox state was less noticeable than in brain mitochondria. In contrast to what we previously reported [35], the present analysis did not reveal an increase in ROS production in *Ttc19*$^{-/-}$ mitochondria. This could be due to experimental differences because in this report we measured ROS production under RET conditions under different respiratory states in isolated mitochondria, whereas in the previous report only basal ROS production was measured, i.e. in the absence of substrates and with different buffer compositions and using different measuring methods.

In conclusion, we believe detailed analyses of the physiological differences in mitochondrial function in different cell types and evaluating the impact of an ETS deficiency on several pathological models will contribute to a greater understanding of the still rather mysterious tissue-specific manifestations of mitochondrial diseases.

Supplementary data to this article can be found online at https://doi.org/10.1016/j.bbadis.2024.167033.

Funding information

This research was funded by: Telethon Foundation/Cariplo Foundation (grant GJC21014 to E.F.-V.), Department of Biomedical Sciences—UNIPD (FERN_FAR22_01 to E.F.-V.), Telethon Foundation (GGP20013 to C.V.), AFM-Téléthon (23706 to C.V.), Associazione Luigi Comini Onlus (MitoFight2, to C.V.), and the Department of Biomedical Sciences—UNIPD (SID2022- VISC_BIRD2222_01 to C.V.), the Medical Research Council (UK) award MC_PC_21046 to establish a National Mouse Genetics Network Mitochondria Cluster (MitoCluster).

The NextGen-O2k project (Oroboros Instruments) has received funding from the European Union's Horizon 2020 research and innovation program under grant agreement No 859770.

CRediT authorship contribution statement

Valeria Balmaceda: Data curation, Formal analysis, Investigation, Methodology, Writing – original draft, Writing – review & editing. **Timea Komlódi:** Formal analysis, Investigation, Methodology, Writing – original draft, Writing – review & editing. **Marten Szibor:** Conceptualization, Methodology, Writing – original draft, Writing – review & editing. **Erich Gnaiger:** Conceptualization, Methodology, Writing – original draft. **Anthony L. Moore:** Conceptualization, Methodology, Supervision, Writing – original draft, Writing – review & editing. **Erika Fernandez-Vizarra:** Conceptualization, Formal analysis, Funding acquisition, Methodology, Supervision, Writing – original draft, Writing – review & editing. **Carlo Viscomi:** Conceptualization, Funding acquisition, Project administration, Supervision, Writing – original draft, Writing – review & editing.

Declaration of competing interest

The authors declare the following financial interests/personal relationships which may be considered as potential competing interests: Carlo Viscomi reports financial support was provided by Telethon Foundation. Carlo Viscomi reports financial support was provided by Associazione Luigi Comini Onlus. Erich Gnaiger reports financial support was provided by European Union. Erika Fernandez-Vizarra reports a relationship with Telethon Foundation that includes: funding grants. EG is founder and CEO of Oroboros Instruments.

Data availability

Original data will be made available on request

References

[1] I. Vercellino, L.A. Sazanov, The assembly, regulation and function of the mitochondrial respiratory chain, Nat. Rev. Mol. Cell Biol. 23 (2022) 141–161.
[2] M. Alcazar-Fabra, F. Rodriguez-Sanchez, E. Trevisson, G. Brea-Calvo, Primary Coenzyme Q deficiencies: a literature review and online platform of clinical features to uncover genotype-phenotype correlations, Free Radic. Biol. Med. 167 (2021) 141–180.
[3] E. Gnaiger, Capacity of oxidative phosphorylation in human skeletal muscle: new perspectives of mitochondrial physiology, Int. J. Biochem. Cell Biol. 41 (2009) 1837–1845.
[4] H. Lemieux, P.U. Blier, E. Gnaiger, Remodeling pathway control of mitochondrial respiratory capacity by temperature in mouse heart: electron flow through the Q-junction in permeabilized fibers, Sci. Rep. 7 (2017) 2840.
[5] M. Gusic, H. Prokisch, Genetic basis of mitochondrial diseases, FEBS Lett. 595 (2021) 1132–1158.
[6] J.B. Stewart, P.F. Chinnery, The dynamics of mitochondrial DNA heteroplasmy: implications for human health and disease, Nat. Rev. Genet. 16 (2015) 530–542.
[7] R.N. Lightowlers, R.W. Taylor, D.M. Turnbull, Mutations causing mitochondrial disease: what is new and what challenges remain? Science 349 (2015) 1494–1499.
[8] T. Klopstock, C. Priglinger, A. Yilmaz, C. Kornblum, F. Distelmaier, H. Prokisch, Mitochondrial disorders, Dtsch. Arztebl. Int. 118 (2021) 741–748.
[9] N.J. Newman, P. Yu-Wai-Man, V. Biousse, V. Carelli, Understanding the molecular basis and pathogenesis of hereditary optic neuropathies: towards improved diagnosis and management, Lancet Neurol. 22 (2023) 172–188.
[10] C. Del Greco, A. Antonellis, The role of nuclear-encoded mitochondrial tRNA charging enzymes in human inherited disease, Genes (Basel) 13 (2022).
[11] W.S. Kunz, Different metabolic properties of mitochondrial oxidative phosphorylation in different cell types—important implications for mitochondrial cytopathies, Exp. Physiol. 88 (2003) 149–154.
[12] D.T. Johnson, R.A. Harris, P.V. Blair, R.S. Balaban, Functional consequences of mitochondrial proteome heterogeneity, Am. J. Phys. Cell Physiol. 292 (2007) C698–C707.
[13] D.T. Johnson, R.A. Harris, S. French, P.V. Blair, J. You, K.G. Bemis, M. Wang, R. S. Balaban, Tissue heterogeneity of the mammalian mitochondrial proteome, Am. J. Phys. Cell Physiol. 292 (2007) C689–C697.
[14] E. Fernandez-Vizarra, J.A. Enriquez, A. Perez-Martos, J. Montoya, P. Fernandez-Silva, Mitochondrial gene expression is regulated at multiple levels and differentially in the heart and liver by thyroid hormones, Curr. Genet. 54 (2008) 13–22.
[15] E. Fernandez-Vizarra, J.A. Enriquez, A. Perez-Martos, J. Montoya, P. Fernandez-Silva, Tissue-specific differences in mitochondrial activity and biogenesis, Mitochondrion 11 (2011) 207–213.
[16] R. Rossignol, M. Malgat, J.P. Mazat, T. Letellier, Threshold effect and tissue specificity. Implication for mitochondrial cytopathies, J. Biol. Chem. 274 (1999) 33426–33432.
[17] R. Rossignol, T. Letellier, M. Malgat, C. Rocher, J.P. Mazat, Tissue variation in the control of oxidative phosphorylation: implication for mitochondrial diseases, Biochem. J. 347 (Pt 1) (2000) 45–53.
[18] G. Benard, B. Faustin, E. Passerieux, A. Galinier, C. Rocher, N. Bellance, J. P. Delage, L. Casteilla, T. Letellier, R. Rossignol, Physiological diversity of mitochondrial oxidative phosphorylation, Am. J. Phys. Cell Physiol. 291 (2006) C1172–C1182.
[19] T. Molinie, E. Cougouilles, C. David, E. Cahoreau, J.C. Portais, A. Mourier, MDH2 produced OAA is a metabolic switch rewiring the fuelling of respiratory chain and TCA cycle, Biochim. Biophys. Acta Bioenerg. 2022 (1863) 148532.
[20] N.P. Lesner, X. Wang, Z. Chen, A. Frank, C.J. Menezes, S. House, S.D. Shelton, A. Lemoff, D.G. McFadden, J. Wansapura, R.J. DeBerardinis, P. Mishra, Differential requirements for mitochondrial electron transport chain components in the adult murine liver, Elife 11 (2022) e80919.
[21] S.P. Burr, F. Klimm, A. Glynos, M. Prater, P. Sendon, P. Nash, C.A. Powell, M. L. Simard, N.A. Bonekamp, J. Charl, H. Diaz, L.V. Bozhilova, Y. Nie, H. Zhang, M. Frison, M. Falkenberg, N. Jones, M. Minczuk, J.B. Stewart, P.F. Chinnery, Cell lineage-specific mitochondrial resilience during mammalian organogenesis, Cell 186 (2023) 1212–1229 (e1221).
[22] K.R. Vinothkumar, J. Zhu, J. Hirst, Architecture of mammalian respiratory complex I, Nature 515 (2014) 80–84.
[23] A.A. Agip, J.N. Blaza, H.R. Bridges, C. Viscomi, S. Rawson, S.P. Muench, J. Hirst, Cryo-EM structures of complex I from mouse heart mitochondria in two biochemically defined states, Nat. Struct. Mol. Biol. 25 (2018) 548–556.
[24] A. Padavannil, M.G. Ayala-Hernandez, E.A. Castellanos-Silva, J.A. Letts, The mysterious multitude: structural perspective on the accessory subunits of respiratory complex I, Front. Mol. Biosci. 8 (2022) 798353.
[25] M.A. Calvaruso, P. Willems, M. van den Brand, F. Valsecchi, S. Kruse, R. Palmiter, J. Smeitink, L. Nijtmans, Mitochondrial complex III stabilizes complex I in the absence of NDUFS4 to provide partial activity, Hum. Mol. Genet. 21 (2012) 115–120.
[26] F. Kahlhofer, K. Kmita, I. Wittig, K. Zwicker, V. Zickermann, Accessory subunit NUYM (NDUFS4) is required for stability of the electron input module and activity of mitochondrial complex I, Biochim. Biophys. Acta Bioenerg. 1858 (2017) 175–181.
[27] M.J.W. Adjobo-Hermans, R. de Haas, P. Willems, A. Wojtala, S.E. van Emst-de Vries, J.A. Wagenaars, M. van den Brand, R.J. Rodenburg, J.A.M. Smeitink, L. G. Nijtmans, L.A. Sazanov, M.R. Wieckowski, W.J.H. Koopman, NDUFS4 deletion triggers loss of NDUFA12 in Ndufs4(−/−) mice and Leigh syndrome patients: a stabilizing role for NDUFAF2, Biochim. Biophys. Acta Bioenerg. 2020 (1861) 148213.
[28] S.E. Kruse, W.C. Watt, D.J. Marcinek, R.P. Kapur, K.A. Schenkman, R.D. Palmiter, Mice with mitochondrial complex I deficiency develop a fatal encephalomyopathy, Cell Metab. 7 (2008) 312–320.
[29] J.D. Ortigoza-Escobar, A. Oyarzabal, R. Montero, R. Artuch, C. Jou, C. Jimenez, L. Gort, P. Briones, J. Muchart, E. Lopez-Gallardo, S. Emperador, E.R. Pesini, J. Montoya, B. Perez, P. Rodriguez-Pombo, B. Perez-Duenas, Ndufs4 related Leigh syndrome: a case report and review of the literature, Mitochondrion 28 (2016) 73–78.
[30] M. Zeviani, C. Viscomi, Mitochondrial neurodegeneration, Cells 11 (2022).
[31] M.A.E. van de Wal, M.J.W. Adjobo-Hermans, J. Keijer, T.J.J. Schirris, J. R. Homberg, M.R. Wieckowski, S. Grefte, E.M. van Schothorst, C. van Karnebeek, A. Quintana, W.J.H. Koopman, Ndufs4 knockout mouse models of Leigh syndrome: pathophysiology and intervention, Brain 145 (2022) 45–63.
[32] S. Corrà, R. Cerutti, V. Balmaceda, C. Viscomi, M. Zeviani, Double administration of self-complementary AAV9NDUFS4 prevents Leigh disease in Ndufs4−/− mice, Brain 145 (2022) 3405–3414.
[33] A. Quintana, S.E. Kruse, R.P. Kapur, E. Sanz, R.D. Palmiter, Complex I deficiency due to loss of Ndufs4 in the brain results in progressive encephalopathy resembling Leigh syndrome, Proc. Natl. Acad. Sci. U. S. A. 107 (2010) 10996–11001.
[34] D. Ghezzi, P. Arzuffi, M. Zordan, C. Da Re, C. Lamperti, C. Benna, P. D'Adamo, D. Diodato, R. Costa, C. Mariotti, G. Uziel, C. Smiderle, M. Zeviani, Mutations in TTC19 cause mitochondrial complex III deficiency and neurological impairment in humans and flies, Nat. Genet. 43 (2011) 259–263.
[35] E. Bottani, R. Cerutti, M.E. Harbour, S. Ravaglia, S.A. Dogan, C. Giordano, I. M. Fearnley, G. D'Amati, C. Viscomi, E. Fernandez-Vizarra, M. Zeviani, TTC19 plays a husbandry role on UQCRFS1 turnover in the biogenesis of mitochondrial respiratory complex III, Mol. Cell 67 (2017) 96–105 (e104).
[36] E. Fernandez-Vizarra, M. Zeviani, Mitochondrial complex III Rieske Fe-S protein processing and assembly, Cell Cycle 17 (2018) 681–687.
[37] J. Koch, P. Freisinger, R.G. Feichtinger, F.A. Zimmermann, C. Rauscher, H. P. Wagentristl, V. Konstantopoulou, R. Seidl, T.B. Haack, H. Prokisch, U. Ahting, W. Sperl, J.A. Mayr, E.M. Maier, Mutations in TTC19: expanding the molecular, clinical and biochemical phenotype, Orphanet J. Rare Dis. 10 (2015) 40.
[38] E. Fernandez-Vizarra, M. Zeviani, Nuclear gene mutations as the cause of mitochondrial complex III deficiency, Front. Genet. 6 (2015) 134.
[39] C. Frezza, S. Cipolat, L. Scorrano, Organelle isolation: functional mitochondria from mouse liver, muscle and cultured fibroblasts, Nat. Protoc. 2 (2007) 287–295.
[40] E. Gnaiger, A.V. Kuznetsov, S. Schneeberger, R. Seiler, G. Brandacher, W. Steurer, R. Margreiter, Mitochondria in the Cold, Springer Berlin Heidelberg, Berlin, Heidelberg, 2000, pp. 431–442.
[41] T. Komlodi, L.H.D. Cardoso, C. Doerrier, A.L. Moore, P.R. Rich, E. Gnaiger, Coupling and pathway control of coenzyme Q redox state and respiration in isolated mitochondria, Bioenerg. Commun. 2021 (2021) 3.
[42] G. Krumschnabel, M. Fontana-Ayoub, Z. Sumbalova, J. Heidler, K. Gauper, M. Fasching, E. Gnaiger, Simultaneous high-resolution measurement of mitochondrial respiration and hydrogen peroxide production, Methods Mol. Biol. 1264 (2015) 245–261.
[43] T. Komlodi, O. Sobotka, G. Krumschnabel, N. Bezuidenhout, E. Hiller, C. Doerrier, E. Gnaiger, Comparison of mitochondrial incubation media for measurement of respiration and hydrogen peroxide production, Methods Mol. Biol. 1782 (2018) 137–155.
[44] S. Miwa, A. Treumann, A. Bell, G. Vistoli, G. Nelson, S. Hay, T. von Zglinicki, Carboxylesterase converts Amplex red to resorufin: implications for mitochondrial H2O2 release assays, Free Radic. Biol. Med. 90 (2016) 173–183.
[45] S.A. Dogan, R. Cerutti, C. Beninca, G. Brea-Calvo, H.T. Jacobs, M. Zeviani, M. Szibor, C. Viscomi, Perturbed redox signaling exacerbates a mitochondrial myopathy, Cell Metab. 28 (2018) 764–775 (e765).
[46] M. Alcazar-Fabra, P. Navas, G. Brea-Calvo, Coenzyme Q biosynthesis and its role in the respiratory chain structure, Biochim. Biophys. Acta 1857 (2016) 1073–1078.
[47] N. Spielmann, C. Schenkl, T. Komlódi, P. da Silva-Buttkus, E. Heyne, J. Rohde, O. V. Amarie, B. Rathkolb, E. Gnaiger, T. Doenst, H. Fuchs, V. Gailus-Durner, M.H. de Angelis, M. Szibor, Knockout of the Complex III subunit Uqcrh causes bioenergetic impairment and cardiac contractile dysfunction, Mamm. Genome 34 (2022) 229–243.

[48] E. Gnaiger, Mitochondrial pathways and respiratory control. An introduction to OXPHOS analysis, in: Bioenerg Commun, 5th ed., 2020.
[49] E.L. Robb, A.R. Hall, T.A. Prime, S. Eaton, M. Szibor, C. Viscomi, A.M. James, M. P. Murphy, Control of mitochondrial superoxide production by reverse electron transport at complex I, J. Biol. Chem. 293 (2018) 9869–9879.
[50] M. Szibor, T. Gainutdinov, E. Fernandez-Vizarra, E. Dufour, Z. Gizatullina, G. Debska-Vielhaber, J. Heidler, I. Wittig, C. Viscomi, F. Gellerich, A.L. Moore, Bioenergetic consequences from xenotopic expression of a tunicate AOX in mouse mitochondria: switch from RET and ROS to FET, Biochim. Biophys. Acta Bioenerg. 1861 (2020) 148137.
[51] E.T. Gibbs, C.A. Lerner, M.A. Watson, H.S. Wong, A.A. Gerencser, M.D. Brand, Site IQ in mitochondrial complex I generates S1QEL-sensitive superoxide/hydrogen peroxide in both the reverse and forward reactions, Biochem. J. 480 (2023) 363–384.
[52] M. Szibor, E. Heyne, C. Viscomi, A.L. Moore, Measuring the mitochondrial ubiquinone (Q) pool redox state in isolated respiring mitochondria, Methods Mol. Biol. 2497 (2022) 291–299.
[53] A.L. Moore, I.B. Dry, J.T. Wiskich, Measurement of the redox state of the ubiquinone pool in plant mitochondria, FEBS Lett. 235 (1988) 76–80.
[54] C. Affourtit, K. Krab, G.R. Leach, D.G. Whitehouse, A.L. Moore, New insights into the regulation of plant succinate dehydrogenase. On the role of the protonmotive force, J. Biol. Chem. 276 (2001) 32567–32574.
[55] S. Raha, B.H. Robinson, Mitochondria, oxygen free radicals, disease and ageing, Trends Biochem. Sci. 25 (2000) 502–508.
[56] C.R. Reczek, N.S. Chandel, ROS-dependent signal transduction, Curr. Opin. Cell Biol. 33 (2015) 8–13.
[57] W.R. Atchley, R. Wei, P. Crenshaw, Cellular consequences in the brain and liver of age-specific selection for rate of development in mice, Genetics 155 (2000) 1347–1357.